Available online at www.sciencedirect.com
SCIENCE DIRECT®
PERGAMON
International Journal of Engineering Science 41 (2003) 1519–1534
International Journal of Engineering Science
www.elsevier.com/locate/ijengsci

Eigenvalue method for computing size effect of cohesive cracks with residual stress, with application to kink-bands in composites

Goangseup Zi [a], Zdeněk P. Bažant [b,*]

[a] *Research Associate, Northwestern University, USA*
[b] *McCormick School Professor and W.P. Murphy Professor of Civil Engineering and Materials Science, Northwestern University, 2145 Sheridan Road, Evanston, IL 60208-3109, USA*

Abstract

The previously developed eigenvalue method for computing the size effect of cohesive crack model is extended to the cohesive crack model with a finite residual stress. In this model, the structure size for which a specified relative length of kink-band corresponds to the maximum load is obtained as an eigenvalue of a homogeneous Fredholm integral equation. This new method is direct and much more efficient than the classical finite element approach in which the entire load-deflection history must be computed to obtain the maximum load. A secondary purpose of the paper is to apply the new method to the effect of structure size on the compressive strength of unidirectional fiber–polymer composites failing by propagation of kink-band with fiber microbuckling. The kink-band is simulated by a cohesive crack model with a linear compressive softening law and a finite residual stress. The simulation shows that the specimens tested have a negative–positive geometry, i.e., the energy release rate of the kink-band for a unit load first decreases but at a certain length of propagation begins to increase. Finally the effect of shape of the softening law of cohesive crack on the size effect curve is studied by using the new eigenvalue method. It is shown that, for a negative–positive geometry, the size effect on the peak load depends on the entire softening curve if the specimens is not too small.

Keywords: Fracture; Size effect; Scaling; Cohesive crack; Composite materials; Compressive failure; Eigenvalue analysis

* Corresponding author. Tel.: +1-847-491-3257; fax: +1-847-491-4011.
E-mail addresses: g-zi@northwestern.edu (G. Zi), z-bazant@northwestern.edu (Z.P. Bažant).

0020-7225/03/$ - see front matter
doi:10.1016/S0020-7225(03)00033-8

1. Introduction

For quasi-brittle materials such as concrete, fiber composites, ice, rocks and tough ceramics, one of the most important practical consequences of fracture mechanics is the size effect. This effect distinguishes fracture mechanics from the classical failure theories based on elasticity and plasticity [11]. Since the early studies of size effect for concrete [2,3], the importance of size effect has become gradually acknowledged for all quasi-brittle materials.

The objective of this paper is twofold: (1) To formulate a new method for computing the size effect curve of cohesive crack model for problems with a finite residual stress—a method that is much more efficient than the classical finite element approach with small load increments, and (2) to demonstrate application of the new method in a study of the size effect due to kink-band propagation in unidirectional fiber composites under compressive loading. Stability of kink-band propagation will also be analyzed and comparisons with the experimental data on size effect in kink-bands will be made.

Recently various fracture mechanics aspects of the kink-band compressive failure of composites came to light. Based on strain measurements at the flank of the kink-band, the experimental studies of Sutcliffe and Fleck [27] and Fleck et al. [16] demonstrated that the axial normal stress across the band decreases with the distance from the kink-band front and reaches a plateau equal to about 50% of the maximum stress. Consequently, the diagram of the axial normal stress versus the axial relative displacement across the kink-band exhibits softening and terminates with a residual yield plateau at about 50% stress reduction. Such crack-like behavior of the band was demonstrated by Fleck et al. [16] and was further confirmed by Moran et al.'s [24] discovery of the phenomenon of band broadening, which is analogous to the increase of crack opening with the distance from the crack tip.

To determine the size effect associated with the kink-band failure of composite materials, Bažant et al. [13] conducted a set of scaled tests using carbon-PEEK specimens. The observed size effect was quite significant. As an extension of the size effect studies in [2–6,10–12], the size effect was described in [13] by an asymptotic size effect formula based on approximations of the J-integral and of the equivalent linear elastic fracture mechanics (LEFM) in which the residual stress of the kink-band was taken into account. The formula was then verified by classical finite element analysis of the cohesive crack growth under small load increments.

2. Eigenvalue analysis of cohesive model with residual stress

2.1. The cohesive crack model

Adapting to concrete the cohesive crack model pioneered by Barenblatt [1], Hillerborg et al. [20], Hillerborg [19] and Petersson [25] analyzed mode I cohesive fracture by condensing out from the structural stiffness matrix all the nodes other than those on the crack line and at the load point. Thus they obtained the compliance matrix (or matrix of Green's function) for the crack surface nodes and the load point (see also Bažant and Planas [11]). The governing equations were then obtained from the crack compatibility condition coupled with the condition of finite stress at the crack tip, which is the same as the condition that the stress intensity factor must vanish.

The energy aspect of the cohesive crack model was studied by Bažant and Li [8,9]. Their energy based stability analysis showed the relation of the crack compatibility condition and the zero stress intensity factor condition to the complementary energy of the structure with cohesive crack. In their formulation, the structure size for which a given relative (dimensionless) crack length corresponds to the maximum load is obtained as the eigenvalue of a homogeneous Fredholm integral equation. This represents an efficient method for calculating the failure loads in which the load-deflection history for a growing cohesive crack need not be calculated.

Bažant and Li's [8,9] eigenvalue method will now be generalized to include a finite residual stress in the cohesive crack, which is a characteristic of kink-bands (as well as mode II shear cracks causing dry-slab snow avalanches or mud slides). When an initial stress σ_0 is present on the crack surfaces, the crack compatibility condition and the condition of zero stress intensity factor (or smooth closure condition) read:

$$w(x) = -\int_{a_0}^{a} C^{\sigma\sigma}(x,x')\sigma(x')\mathrm{d}x' - \sigma_0 C^{\sigma 0}(x) + \sigma_{\mathrm{N}} C^{\sigma \mathrm{N}}(x) \tag{1}$$

$$\int_{a_0}^{a} k(x')\sigma(x')\mathrm{d}x' + k^0(a)\sigma_0 + k^{\mathrm{N}}(a)\sigma_{\mathrm{N}} = 0 \tag{2}$$

where x = coordinate along the kink-band, w = crack opening displacement, a = length of cohesive crack, a_0 = length of the initial notch (or stress-free crack), $C^{\sigma\sigma}(x,x')$, $C^{\sigma 0}(x)$, $C^{\sigma \mathrm{N}}(x)$ = compliances of the structure, σ_{N} = nominal stress (= load divided by D and by unit thickness), σ = stress on cohesive crack, and $k(x)$, k^0, k^{N} = stress intensity factors for unit loads. For the sake of generality, we consider, with no significant complication, a more general case where the faces of preexisting crack may be loaded by uniform fluid pressure σ_0 (Fig. 1). In the case of notched specimens, we of course have $\sigma_0 = 0$.

Eq. (1) is the condition that the crack opening indicated by the softening stress–displacement law must be compatible with the elastic deformation of the structure and Eq. (2) is the condition

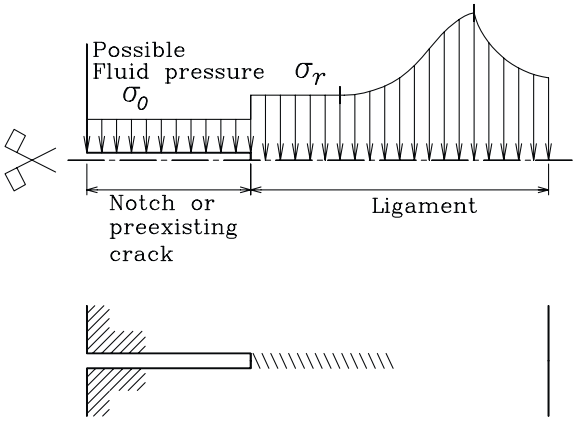

Fig. 1. Sketch of stress distribution along cohesive crack.

that the stress intensity factor at the crack tip must vanish (because the stress must be finite). Note that $C^{\sigma 0}(x) = \int_0^{a_0} C^{\sigma\sigma}(x, x')\mathrm{d}x'$. For the sake of simplicity of calculation, the kink-band is simulated as a crack running orthogonally to the fibers.

2.2. Dimensionless formulation

We introduce dimensionless variables defined as

$$\begin{aligned}
&\xi = x/D, \quad \overline{D} = \sigma_f D/Ew_c = D/2l_{ch}, \quad \bar{w} = w/w_c,\\
&\alpha = a/D, \quad \alpha_0 = a_0/D,\\
&\overline{C}^{\sigma\sigma} = EbC^{\sigma\sigma}, \quad \overline{C}^{0} = C^{0}E/D, \quad \overline{C}^{N} = C^{N}E/D,\\
&\bar{k} = k\sqrt{D}, \quad \bar{k}^{0} = k^{0}/\sqrt{D}, \quad \bar{k}^{N} = k^{N}/\sqrt{D},\\
&\overline{\sigma} = \sigma/\sigma_f \quad \overline{\sigma}_0 = \sigma_0/\sigma_f, \quad \overline{\sigma}_N = \sigma_N/\sigma_f
\end{aligned} \tag{3}$$

Here D = characteristic size of structure, ξ = dimensionless coordinate along the kink-band, $\overline{D}$ = dimensionless structure size, $l_{ch} = Ew_c/2\sigma_f$ = constant analogous to Irwin's characteristic length in the case of a triangular softening law with zero residual stress, σ_f = material strength, w = dimensionless crack opening displacement, w_c = critical opening displacement at which the cohesive stress attains the final residual stress value, $\overline{\sigma}$ = dimensionless cohesive stress, α_0 = dimensionless length of notch, α = dimensionless length of cohesive crack (or kink-band), $\overline{C}^{N}$ = dimensionless compliance corresponding to the dimensionless nominal stress $\overline{\sigma}_N$, $\overline{C}^{0}$ = compliance corresponding to the dimensionless initial uniform stress $\overline{\sigma}_0$ applied on the faces of a preexisting crack in the interval $[0, \alpha_0]$, $\overline{C}^{\sigma\sigma}$ = compliance for concentrated force pair applied on the crack faces, i.e., $\bar{w}$ at ξ caused by a unit stress $\overline{\sigma}$ applied at ξ', and $\bar{k}$, $\bar{k}^0$ and $\bar{k}^N$ = dimensionless stress intensity factors due to unit value of the corresponding stresses or forces (e.g. Bažant and Planas [11]).

Upon substituting the dimensionless variables into (1) and (2), one obtains the following dimensionless formulation of the cohesive crack model:

$$\bar{w}(\xi) = -\overline{D}\int_{\alpha_0}^{\alpha} \overline{C}^{\sigma\sigma}(\xi, \xi')\overline{\sigma}(\xi')\mathrm{d}\xi' - \overline{D}\overline{\sigma}_0\overline{C}^{\sigma 0}(\xi) + \overline{D}\overline{\sigma}_N\overline{C}^{\sigma N}(\xi) \tag{4}$$

$$\int_{\alpha_0}^{\alpha} \bar{k}(\xi')\overline{\sigma}(\xi')\mathrm{d}\xi' + \bar{k}^0\overline{\sigma}_0 + \bar{k}^N\overline{\sigma}_N = 0 \tag{5}$$

The terms $\overline{D}\overline{\sigma}_0\overline{C}^{\sigma 0}(\xi)$ and $\bar{k}^0\overline{\sigma}_0$ in (4) and (5) take into account the possible initial uniform stress (fluid pressure) on the faces of a preexisting crack (for a notch, $\overline{\sigma}_0 = 0$). Note that these terms would not need to be included if the integral spanned the range $[0, \alpha]$ rather than $[\alpha_0, \alpha]$, in which case the stress step at the notch tip would have to be considered in the integration. The general equations would then be more compact. However, inclusion of these terms is convenient for the eigenvalue formulation in the next section.

To obtain the entire load-deflection curve, the discrete forms of Eqs. (4) and (5) may be solved for subsequent small loading increments as the crack grows along the assumed crack path. For each loading step, the problem is reduced to a linear matrix equation. The computation is most efficient and accurate if one prescribes the crack tip location at subsequent nodal points and solves the corresponding load and the load-point displacement. The condition of zero-stress intensity factor is satisfied by setting the stress at the cohesive crack tip equal to the given finite material strength σ_f. To obtain a compact form, the integration range may be taken as $[0,\alpha]$, and then the discrete form of (4) is

$$\{\bar{\mathbf{w}}\} + \overline{D}\left[\overline{\mathbf{C}}^{\sigma\sigma}\right][\mathbf{T}]\{\overline{\sigma}\}\Delta\xi = \overline{D}\overline{\sigma}_{\mathrm{N}}\left\{\overline{\mathbf{C}}^{\sigma\mathrm{N}}\right\} \tag{6}$$

where $[\mathbf{T}]$ is a tridiagonal matrix characterizing the stress distribution [21]. To solve (6), the matrix equation is divided into two parts: the completely separated cracked zone in which the surface traction is known, and the failure process zone in which the stress–displacement relation (the softening law) is known. For the detailed solution procedure, see e.g. Bažant and Planas (Section 7.4.3 [11]).

2.3. Reduction to eigenvalue problem

Using the aforementioned classical analysis in which small crack advances are analyzed, the computation of the size effect curve from the discrete crack compatibility condition (6) is a time consuming process, since the entire load-deflection history must be calculated for each specimen size. A much more efficient approach is provided by the discrete formulations of Li and Hong [22], Li and Liang [23], and Li and Bažant [21] and the subsequent continuous energy-based reformulation of Bažant and Li [8,9]. In this approach, computation of the load-deflection history is bypassed by formulating the problem of maximum load as an eigenvalue problem.

To express the conditions of continuing equilibrium and compatibility, we start by differentiating the dimensionless integral crack compatibility condition (4);

$$\begin{aligned}\bar{w}_{,\alpha} = -\overline{D}\int_{\alpha_0}^{\alpha}\left[\overline{C}^{\sigma\sigma}_{,\alpha}(\xi,\xi')\overline{\sigma}(\xi') + \overline{C}^{\sigma\sigma}(\xi,\xi')\overline{\sigma}_{,\alpha}(\xi')\right]\mathrm{d}\xi' - \overline{D}\overline{C}^{\sigma\sigma}(\xi,\alpha)\overline{\sigma}(\alpha) - \overline{D}\overline{\sigma}_0\overline{C}^{\sigma 0}_{,\alpha}(\xi)\\ + \overline{D}\overline{\sigma}_{\mathrm{N}}\overline{C}^{\sigma\mathrm{N}}_{,\alpha}(\xi) + \overline{D}\frac{\partial\overline{\sigma}_{\mathrm{N}}}{\partial\alpha}\overline{C}^{\sigma\mathrm{N}}(\xi)\end{aligned} \tag{7}$$

where the third term and the last term are recognized to be zero because $\overline{C}(\xi,\alpha) = 0$ (i.e., the opening at crack tip vanishes) and because, at maximum load, $\mathrm{d}\overline{\sigma}_{\mathrm{N}}/\mathrm{d}\alpha = 0$. In the derivation, we will need the following well-known relations between the compliance derivatives and the stress intensity factors [11,28] used by Bažant and Li [8];

$$\frac{\partial\overline{C}^{\sigma\mathrm{N}}}{\partial\alpha} = -2\bar{k}(\xi)\bar{k}^{\mathrm{N}} \tag{8}$$

$$\frac{\partial\overline{C}^{\sigma 0}}{\partial\alpha} = 2\bar{k}(\xi)\bar{k}^{0} \tag{9}$$

$$\frac{\partial \overline{C}^{\sigma\sigma}(\xi,\xi')}{\partial \alpha} = 2\bar{k}(\xi)\bar{k}(\xi') \tag{10}$$

Substitution into (7) furnishes

$$\bar{w}_{,\alpha} = -\overline{D}\int_{\alpha_0}^{\alpha} \overline{C}^{\sigma\sigma}(\xi,\xi')\overline{\sigma}_{,\alpha}(\xi')\,\mathrm{d}\xi' - 2\overline{D}\bar{k}(\xi)\left[\int_{\alpha_0}^{\alpha} \bar{k}(\xi')\overline{\sigma}(\xi')\mathrm{d}\xi' + \bar{k}^0\overline{\sigma}_0 + \bar{k}^{\mathrm{N}}\overline{\sigma}_{\mathrm{N}}\right] \tag{11}$$

The last (bracketed) term of this equation vanishes because of the condition of zero-stress intensity factor (5). Thus Eq. (11) simplifies to the following homogeneous Fredholm integral equation:

$$-\int_{\alpha_0}^{\alpha} \overline{C}^{\sigma\sigma}(\xi,\xi')\overline{\sigma}_{,\bar{w}}(\xi')\bar{w}_{,\alpha}(\xi')\mathrm{d}\xi' = \frac{1}{\overline{D}}\bar{w}_{,\alpha}(\xi) \tag{12}$$

Same as Bažant and Li [8], the inverse of $1/\overline{D}$ of the dimensionless size $\overline{D}$ for which a specified relative crack length $\overline{\alpha}$ corresponds to the maximum load is an eigenvalue of this equation and $\bar{w}_{,\alpha}$ is the eigenfunction. It can further be shown [9] that $1/\overline{D}$ is the first eigenvalue. Eq. (12) is a continuous version of the discrete eigenvalue formulation of Li and Bažant [21], which was derived indirectly by matrix manipulation from the stability limit of potential energy (and without the need for the zero-stress intensity factor condition and the relations (8)–(10)). When (12) is discretised, $\overline{\sigma}_{,\bar{w}}$ becomes a diagonal matrix and $\bar{w}_{,\alpha}$ the eigenvector. Note that the initial stress σ_0 and the residual stress σ_{r} do not affect the eigenvalue of the cohesive crack because $\overline{\sigma}_{,\alpha} = \bar{s}_{,\alpha}$, where $\bar{s}(x) = \overline{\sigma}(x) - \overline{\sigma}_{\mathrm{r}}$ denotes the cohesive stress in excess of the residual stress, i.e., $\overline{\sigma}(x) = \bar{s}(x) + \overline{\sigma}_{\mathrm{r}}$ = total cohesive stress.

The nominal strength $\overline{\sigma}_{\mathrm{N}}$ can be obtained from the crack compatibility condition (4). To this end, (4) may be multiplied by $\overline{\sigma}_{,\bar{w}}(\xi)\bar{w}_{,\alpha}(\xi)$ and integrated over the interval $[\alpha_0,\alpha]$;

$$\begin{aligned}\int_{\alpha_0}^{\alpha} \bar{w}(\xi)\overline{\sigma}_{,\bar{w}}(\xi)\bar{w}_{,\alpha}(\xi)\mathrm{d}\xi = {} & \int_{\alpha_0}^{\alpha} \sigma(\xi)\left[-\overline{D}\int_{\alpha_0}^{\alpha} \overline{C}^{\sigma\sigma}(\xi',\xi)\overline{\sigma}_{,\bar{w}}(\xi)\bar{w}_{,\alpha}(\xi)\mathrm{d}\xi\right]\mathrm{d}\xi' \\ & - \overline{D}\overline{\sigma}_0\int_{\alpha_0}^{\alpha} \overline{C}^{\sigma 0}(\xi)\overline{\sigma}_{,\bar{w}}(\xi)\bar{w}_{,\alpha}(\xi)\mathrm{d}\xi \\ & + \overline{D}\overline{\sigma}_{\mathrm{N}}\int_{\alpha_0}^{\alpha} \overline{C}^{\sigma \mathrm{N}}(\xi)\overline{\sigma}_{,\bar{w}}(\xi)\bar{w}_{,\alpha}(\xi)\mathrm{d}\xi \qquad (13) \\ = {} & \int_{\alpha_0}^{\alpha} \sigma(\xi)\bar{w}_{,\alpha}(\xi')\mathrm{d}\xi' - \overline{D}\overline{\sigma}_0\int_{\alpha_0}^{\alpha} \overline{C}^{\sigma 0}(\xi)\overline{\sigma}_{,\bar{w}}(\xi)\bar{w}_{,\alpha}(\xi)\mathrm{d}\xi \\ & + \overline{D}\overline{\sigma}_{\mathrm{N}}\int_{\alpha_0}^{\alpha} \overline{C}^{\sigma \mathrm{N}}(\xi)\overline{\sigma}_{,\bar{w}}(\xi)\bar{w}_{,\alpha}(\xi)\mathrm{d}\xi \qquad (14)\end{aligned}$$

where the integration variables ξ and ξ' are interchanged in the second term of (13). From this relation, the dimensionless nominal strength is obtained as

$$\overline{\sigma}_{\mathrm{N}} = \frac{\int_{\alpha_0}^{\alpha} \bar{w}_{,\alpha}(\xi)\left\{\overline{\sigma}_{,\bar{w}}(\xi)\bar{w}(\xi) - \overline{\sigma}(\xi)\right\}\mathrm{d}\xi + \overline{D}\overline{\sigma}_0 \int_{\alpha_0}^{\alpha} \overline{C}^{\sigma 0}(\xi)\overline{\sigma}_{,\bar{w}}(\xi)\bar{w}_{,\alpha}(\xi)\mathrm{d}\xi}{\overline{D}\int_{\alpha_0}^{\alpha} \overline{C}^{\sigma \mathrm{N}}(\xi)\overline{\sigma}_{,\bar{w}}(\xi)\bar{w}_{,\alpha}(\xi)\mathrm{d}\xi} \tag{15}$$

When the softening law of cohesive crack up to the critical opening displacement w_{c} is linear, Eq. (15) can be further simplified. For the linear softening law with zero residual stress, we have

$$\overline{\sigma}_{,\bar{w}} = -1, \quad \bar{w} + \overline{\sigma} = 1 \tag{16}$$

and then Eq. (15) reduces to the expression

$$\overline{\sigma}_{\mathrm{N}} = \frac{-\int_{\alpha_0}^{\alpha} \bar{w}_{,\alpha}(\xi)\mathrm{d}\xi + \overline{D}\overline{\sigma}_0 \int_{\alpha_0}^{\alpha} \overline{C}^{\sigma 0}(\xi)\bar{w}_{,\alpha}(\xi)\mathrm{d}\xi}{\overline{D}\int_{\alpha_0}^{\alpha} \overline{C}^{\sigma \mathrm{N}}(\xi)\bar{w}_{,\alpha}(\xi)\mathrm{d}\xi} \tag{17}$$

Note that the Eq. (17) applies only to positive geometries (i.e., the geometries of structure and loading such that the stress intensity factor for constant load increases as the crack propagates). The reason is that, for the negative–positive geometries, the fracture process zone (FPZ) can get fully developed before reaching the maximum load, i.e., the case $\overline{\sigma}_{,\bar{w}} = 0$ when $w > w_{\mathrm{c}}$ can be attained. However, Eqs. (12) and (15) are valid for both positive geometries and negative–positive geometries since the eigenfunction of (12), $\mathrm{d}\overline{\sigma}/\mathrm{d}\bar{w}$, is finite for all smooth softening laws. The effect of the residual stress acting on the notch faces is included in expression (15) for the nominal strength.

Because (12) is the continuous version of Li and Bažant's [21] discrete formulation, almost the same algorithm as in that work may be used to obtain the size effect. With a slight improvement, the algorithm is as follows.

(1) Prescribe the location of the cohesive crack tip α at successive nodes on the crack path.
(2) Estimate the eigenvalue of Eq. (12) corresponding to the dimensionless size $\overline{D}$ (the estimate can simply be the value in the previous step).
(3) Compute the dimensionless opening $\bar{w}$ and $\mathrm{d}\overline{\sigma}/\mathrm{d}\bar{w}$ from the crack compatibility condition (4) or (6) for the current relative crack length.
(4) Solving the eigenvalue problem (12), compute the dimensionless size $\overline{D}$ using the values of $\bar{w}$ and $\mathrm{d}\overline{\sigma}/\mathrm{d}\bar{w}$ obtained in the step 3. The first eigenvalue is taken as $1/\overline{D}$ [9].
(5) Compute the dimensionless nominal strength $\overline{\sigma}_{\mathrm{N}}$ by (15).
(6) Repeat steps 3–5 until $\overline{D}$ converges, according to a specified tolerance.
(7) Calculate and output the actual size $D = Ew_{\mathrm{c}}\overline{D}/\sigma_{\mathrm{f}}$ and the corresponding actual nominal strength $\sigma_{\mathrm{N}} = \sigma_{\mathrm{f}}\overline{\sigma}_{\mathrm{N}}$.
(8) Return to the step 2 and start the analysis for the next dimensionless crack length α.

All the computations are of course conducted in a discrete form corresponding to the chosen nodal subdivisions of the crack path. In the discrete form, the integrals are approximated by sums and thus (12) becomes a matrix eigenvalue problem, which is then solved by a standard linear algebra subroutine.

3. Application to previous size effect tests of kink-band failure

3.1. Test description

The eigenvalue method just formulated will now be applied to the analysis of the size effect on the compressive strength of fiber composites failing by kink-band propagation. First it is necessary to review the recent experimental investigation of Bažant et al. [13]. In this investigation, the growth of kink-band was stabilized by providing a rotation restraint of specimen ends. The restraint allowed the kink-band to grow stably, under increasing load, for a considerable distance. This means that the specimens have a negative–positive geometry, i.e., a geometry for which the derivative of the stress intensity factor for a unit load with respect to the kink-band length is first negative and later changes to positive.

To exclude the effect of random variation of material strength over the specimen volume (known to cause Weibull-type size effect), the specimens (shown in Fig. 2(a) and (b)) were provided with notches. The notches ensured the failure to begin in one desired place, preventing the failure from starting at diverse locations at which the material may be statistically the weakest. To avoid bifurcation of the equilibrium path due to asymmetric propagation [7], a one-sided notch (on which $\sigma_0 = 0$) was introduced instead of two symmetric notches.

The kink-band failure is often combined with axial splitting-shear cracks and delaminations. Such combined failures are difficult to analyze because the contributions of the microbuckling and of the shear-splitting delamination failures in the kink-band are not easy to separate. It was found that this problem can be eliminated by making the starter notch inclined (Fig. 2(b)), with the same angle as that preferred by a long out-of-plane kink-band. This inclination was found by trial tests to be about 25.4°. This novel experimental feature made it possible to eliminate in most tests the axial splitting-shear cracks and thus obtain pure kink-band failures.

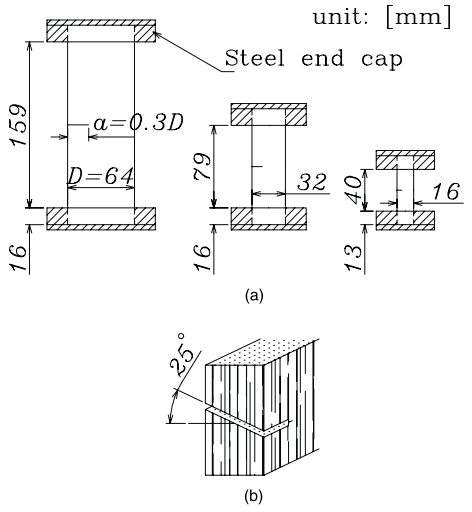

Fig. 2. (a) Geometrically similar single edge notched carbon-PEEK specimens tested, and scheme of loading, and (b) transversely slanted notches used in tests, achieving pure kink-band failure (Bažant et al. [13]).

The test specimens are shown in Fig. 2(a). They were scaled in two dimensions, in the ratio 1:2:4, the thickness b in the third dimension being kept constant. The specimens had the thickness $b = 12.3$ mm, and were made of 100 plies. The end caps were glued by epoxy. A notch of length $a_0 = 0.3D$ (where D is the specimen width, taken as the characteristic dimension of specimens) was machined in each specimen, using a banded diamond blade saw. The detailed fabrication procedure of the specimens is described in Bažant et al. [13].

After the specimens had been cut from the molded sheets, they were provided with massive end caps (made of 1040 hot rod steel), to which they were glued by epoxy. An extra length of the specimen beyond the similarity length (whose effect will be discussed later) was provided in order to allow embedment of specimen ends within the end caps (Fig. 2(a)). The end caps were restrained so as to prevent any end rotations. All the specimens were tested under a controlled stroke rate. After the kink-band had initiated at the notch tip, it was seen to propagate stably on both the front and back sides of the specimen.

Fig. 3 shows the nominal strength σ_N versus the size D. If there were no size effect, as currently assumed in design and exhibited by all the existing formulae for the kink-band stress expressed in terms of stress or strain, the plot in Fig. 3 would have to be horizontal. Any theory based on plasticity, or any theory in which failure is indicated by some critical values of stress or strain, predicts a horizontal plot. In the tests, however, the trend was clearly seen to be downward. So, despite the use of PEEK matrix, which is relatively ductile, the size effect for these large, albeit not extremely large, specimens is strong.

One of the small specimens, corresponding to the highest peak load in Fig. 3 (shown as an empty circle), did not develop a kink-band across the specimen but failed by a vertical shear crack that started from the notch tip and produced axial splitting. Inclusion of this specimen in the analysis is, therefore, questionable. In the previous work [13], the data point for this specimen was nevertheless included because of the argument that the failure load corresponding to a pure kink-band mechanism could not have been smaller than the measured load. However, a later examination revealed a rather anomalous shape of the load-deflection diagram for this particular

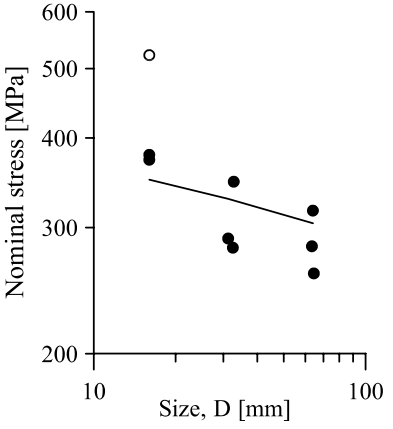

Fig. 3. Results of the tests of nominal strength of carbon-PEEK specimens tested; test data (symbols), in which the empty circle represents the specimen failed by shear splitting, and fitting by the cohesive crack model (solid line).

specimen, indicating that some of the test conditions were not controlled properly. Therefore, this data point (the empty circle in Fig. 3) is here deleted from the analysis.

The diagrams of the applied load P versus the stroke of the piston for the individual specimens are shown in Fig. 4(bottom). All these load-deflection diagrams exhibit post-peak softening rather than a horizontal yield plateau at peak load. This fact alone suffices to demonstrate that a fracture-type approach is required. Furthermore, these diagrams exhibit a terminal yield plateau, which confirms the existence of a finite residual stress across the kink-band.

The larger the scatter of test results, the broader must be the size range of test specimens needed to determine the size effect. The scatter of the results in Fig. 3 is quite large. This is, however, typical of compression failure of fiber composites (because of microbuckling and its strong sensitivity to fiber misalignment; [14,15]). In view of the scatter, the size range of 1:4 appeared just about the minimum for being able to clearly demonstrate the size effect (to reduce the relative width of the scatter band, the ratio of the sizes of the smallest and largest specimens should be increased in future testing).

Compared to the case of loading through a pin, which would allow free rotations at the ends, the present boundary condition of restraint against rotation complicates the test evaluation because a statically indeterminate bending moment develops at the ends, causing the compression resultant to shift laterally during kink-band propagation. However, the end restraint has the advantage that the test becomes much more stable. This made it possible (1) to demonstrate that a

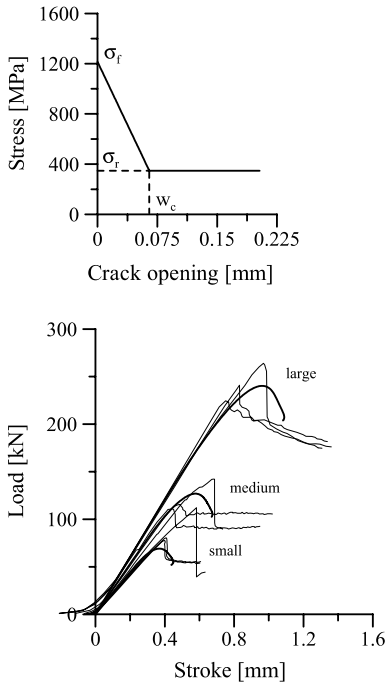

Fig. 4. The optimum fit of the test data by the numerical analysis with the cohesive crack model; the triangular softening law determined (top) and the load-deflection diagrams simulated versus experimental results (bottom) in which the thin lines represent the test data and the thick lines the simulations by the cohesive crack model.

stable propagation of a long kink-band is possible (which had been doubted by previous researchers), (2) to observe the post-peak deformations well beyond the peak load, and (3) to approach the residual stress plateau and observe the residual stress (Fig. 3).

3.2. Identification of model parameters from test data

Aside from the program for the eigenvalue analysis of the size effect, a computer program for computing the entire load-deflection history for a cohesive crack with residual stress has also been written. The calculation of load-deflection history is based on solving the discrete form of the crack compatibility condition (6).

It is appropriate to discuss the role of the extra length of embedment of test specimens into the end caps, which was neglected in the previous analysis by Bažant et al. [13]. This extra length, which was needed to attach the massive end cap to each specimen (Fig. 2(a)), did not adhere to geometric similarity of specimens of different sizes. If the dissimilar extra length were sufficiently small, the effect of embedment would have been negligible. But this was not the case. Whether or not the effect of such embedment is negligible can be checked by comparing the initial slopes of the measured curves of P versus displacement u (or nominal strength σ_N versus dimensionless displacement $\bar{u} = u/L$). Since there is no size effect in linear elasticity, these initial slopes would have been identical for all the specimens if the deformation in the dissimilar embedment were negligible. However, these initial slopes are seen (in Fig. 4(bottom)) to be quite different when all the data are plotted together. It follows that geometrical similarity does not hold.

Because of the lack of similarity, different compliance matrices are needed for the three sizes (or geometries) tested. The aspect ratios of the specimens including the embedment length are 1:3.00 for the large size, 1:3.47 for the medium size, and 1:4.12 for the small size (Fig. 2(a)). The corresponding compliance matrices were computed by two-dimensional elastic finite element analysis. In view of symmetry, only a half of each specimen was modeled. Because of the superior stiffness of the end caps (Fig. 5), the embedded portion of each specimen was assumed to be in the state of plane strain, while the rest of each specimen was considered to be in the state of plane stress.

For the sake of simplicity, the softening law was assumed to be linear (triangular) up to the critical crack opening displacement w_c (Fig. 4(top)). Although other softening laws, such as a

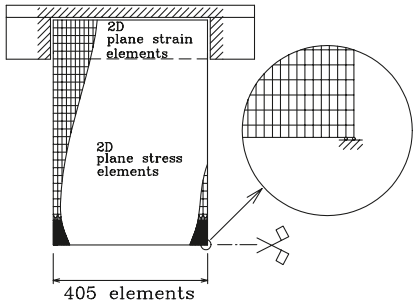

Fig. 5. The two dimensional finite element mesh for the calculation of the compliance matrices and the boundary conditions.

bilinear law or an exponential law, could be considered, the data fits would be expected to be equally good since the scope of data is limited.

From the test data, the residual stress σ_r has been easily identified as a uniform stress balancing the final residual force carried by the specimen at the end of test; $\sigma_r = 347$ MPa. As for the softening law, Guinea et al. [17,18] showed that its determination from the size effect tests alone is an ill-conditioned problem. But this is true only for positive geometries, for which the maximum load depends almost exclusively on the initial slope of the softening law. Since the present specimens represent a negative–positive geometry, identification of the remaining two parameters, the compressive strength σ_f and the critical crack opening displacement w_c, has been possible. It has been done by optimum fitting of the entire load–deflection histories of the individual specimens to the test data (Fig. 4(bottom)). This provided the compressive strength of $\sigma_f = 1,216$ MPa, and the critical crack opening displacement of $w_c = 0.06$ mm (Fig. 4(top)), while the Young's modulus was $E = 7.20$ GPa.

3.3. Neglect of out-of-plane displacement in the kink

The microbuckling of compressed fibers in the kink-band [14] happens in the out-of-plane direction, making the deformation of specimen three-dimensional. Then why don't we need a three-dimensional finite element program?

The reason can be explained by a simple estimation based on beam theory. For the sake of simplicity, we imagine narrow vertical strips of the specimen to act independently, like beams that are fixed at the end caps and bend in the out-of-plane direction (Fig. 6(b)). The kink-band width, denoted as 2δ (and measured as 1.5 mm) is a constant, representing a property of the composite. Neglecting the out-of-plane bending moment in the beam at the kink-band face, we have a cantilever fixed at the end cap. The out-of-plane displacement at the kink is $w = \delta \sin\vartheta$ where $\vartheta =$ fiber inclination in the kink when the axial stress in the kink-band is reduced to the residual value σ_r ($\vartheta \approx 45°$, as seen in experiments). This causes out-of-plane forces on the kink-band,

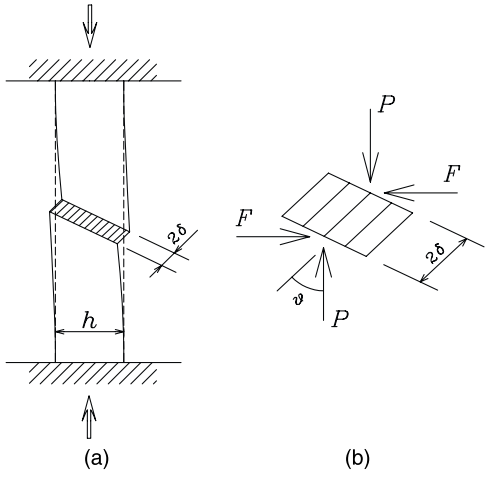

Fig. 6. (a) Out-of-plane deformation of a unidirectional composite which fails by compression and (b) force equilibrium of the kink-band.

$F = 3(Eh^3/12)(\delta \sin\vartheta)/L^3$, where L, h = half-length and thickness of specimen respectively. Based on the moment equilibrium condition of an element of the kink-band, the axial force required to balance force F is

$$\Delta P = F(\delta\cos\vartheta)/(\delta\sin\vartheta) \quad \text{or} \quad \Delta P = E\delta\cos\vartheta\, h^3/4L^3 \tag{18}$$

For the specimens of the smallest size, one thus gets corrections $\Delta P \approx 104$–147 N/mm, which is less than 3% of the maximum axial force and thus insignificant. For the longer specimens, the correction is much less, since $\Delta P \propto L^{-3}$. Therefore, the effect of out-of-plane forces can be neglected.

3.4. Development of failure process zone and size effect

In LEFM, the axially loaded prismatic fracture specimen with a one-sided notch is known to represent a positive geometry [11], i.e., the stress intensity factor for unit load increases with the crack length. However, this is true only if the specimen is sufficiently slender, or if the ends are free to rotate. The present specimens, though, represent, a negative geometry, i.e., the stress intensity factor for unit load initially decreases. The negative geometry is useful for achieving a more stable response, as well as for exploring the entire softening curve.

Because of the rotational restraint, the location of the axial load resultant is statically indeterminate and its location shifts away from the center during loading. Consequently, the loading for different specimen sizes and the kink-band lengths at maximum loads are not geometrically similar. This means that corrections need to be introduced into the simple size effect law for positive geometries. These corrections have been worked out, on the basis of equivalent LEFM [13], but a compact simple formula does not exist.

The computed stress profiles across the smallest specimen at $P_{\max}$ are plotted for three stages of loading in Fig. 7. The maximum load $P_{\max}$ for positive geometries depends only on the initial segment of the softening stress–displacement curve of the cohesive crack model [17,18,26]. The reason is that, for positive geometries, the stress at the notch tip at $P_{\max}$ is still above the tail

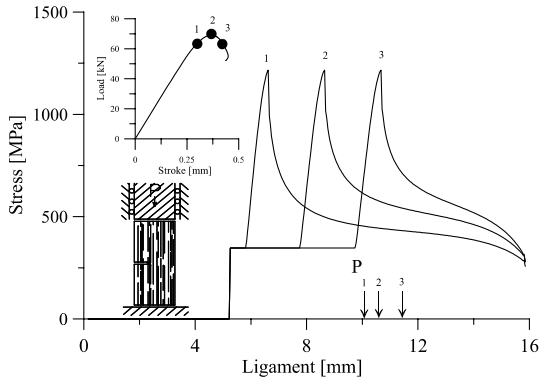

Fig. 7. Stress profiles along the width of the carbon-PEEK specimens before, at and after the maximum load in the small specimen, which is chosen for better graphical resolution.

portion of the softening curve. For negative geometries, however, this is not true, and the stress profiles in Fig. 7 confirm it.

The profiles in Fig. 7 were computed by solving, under the assumption of linear softening up to the residual stress plateau, the compatibility condition of crack band formulated in terms of the compliance matrices. The solutions were computed for subsequent small increments of the displacement at the top of specimen. The maximum loads obtained by this much more tedious analysis agreed with those calculated by the present eigenvalue approach (e.g. Fig. 8(c)), which provided a check on the correctness of this approach.

In the computed profiles, one can see the location of the FPZ during the loading process. Further one should note that the locations of the compression resultant at P_{max} for the three specimen sizes are dissimilar, which was shown already in Bažant et al. [13]. For the small size specimen, the location of this resultant is shown in Fig. 7 by arrow 2. Aside from the embedment length, this is another reason for geometrical dissimilarity among the three sizes, which was already taken into account in the previous work [13].

The fact that the geometry is initially negative is manifested by the fact that the FPZ (i.e., the zone of softening) becomes detached from the notch tip before P_{max} is reached. But this is generally true only if the specimen is not too small. Fig. 7 demonstrates that this situation is achieved, i.e., the residual stress value is attained at P_{max}, even for the smallest specimen. This fact is the reason why P_{max} is influenced not only by the initial portion of the softening curve, as in normal fracture specimens, but by the entire softening curve.

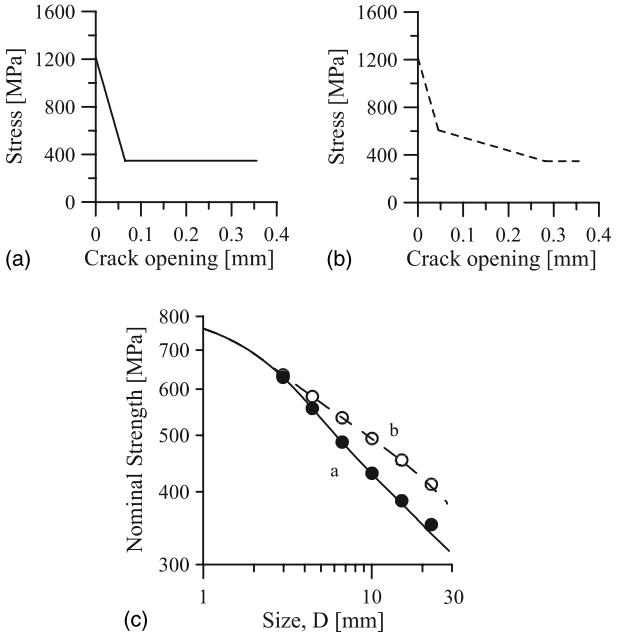

Fig. 8. (a) The triangular softening law determined by the data fitting, (b) a bilinear softening law chosen with the same initial slope as the triangular one and (c) the size effects corresponding to the two softening laws, in which the solid line is for the former, the dashed line is for the latter and the symbols represent nominal strengths obtained by the classical method.

The size effect curves, shown in Fig. 8(c), were alternatively computed (by the present eigenvalue method) also for the case of the bilinear softening law shown in Fig. 8(b), for which the initial tangent is the same as for the linear softening law (Fig. 8(a)). The solid size effect curves in Fig. 8(c) are for the linear law, the dashed for bilinear. As expected, both size effect curves coincide for small sizes, but deviate significantly at large sizes.

The calculations confirm that, for specimens of negative–positive geometry such as the present ones, the maximum load depends not only on the initial segment of the softening curve of the cohesive crack model (as is the case for positive geometry specimens) but on the entire softening curve. However, the case of very small specimens is an exception because the softening at maximum load does not attain the residual stress value.

The fact that the stress at notch tip is reduced to σ_r also implies that the size effect curve must be affected by the total fracture energy corresponding to the area under that softening curve and above the residual stress line.

4. Conclusions

(1) The eigenvalue method for calculating the maximum loads for the cohesive crack model is extended to softening stress–displacement curves that terminate with a finite residual stress. The eigenvalue of the cohesive crack is characterized by the excess of the residual stress. The residual stress or the initial stress on the notch does not affect it.
(2) The proposed extended method allows an efficient calculation of the size effect curves of the cohesive crack model with residual stress, for both positive and negative–positive geometries.
(3) Application of the cohesive crack method to kink-band failure of unidirectional fiber composites yields good agreement with the previous measurements.
(4) The results demonstrate that the size effect for negative–positive geometries is affected not only by the initial tangent of the softening curve but by the entire softening curve of cohesive crack. However, this does not need to hold true for very small sizes.

Acknowledgement

Thanks are due to the Office of Naval Research for partially supporting this research under Grant N00014-91-J-1109 to Northwestern University monitored by Dr. Y.D.S. Rajapakse.

References

[1] G.I. Barenblatt, The mathematical theory of equilibrium of cracks in brittle fracture, Adv. Appl. Mech. 7 (1962) 55–129.
[2] Z.P. Bažant, Instability, ductility, and size effect in strain-softening concrete, J. Eng. Mech. Div. ASCE 102 (EM2) (1976) 331–344, disc. 103, 357–358, 775–777, 104, 501–502.
[3] Z.P. Bažant, Size effect in blunt fracture: Concrete, rock, metal, J. Eng. Mech. ASCE 110 (1984) 518–535.
[4] Z.P. Bažant, Size effect on structural strength: A review, Archives of Applied Mechanics (Ingenieur Archiv) 69 (1999) 703–725.

[5] Z.P. Bažant, Scaling of structural strength, Hermes-Penton, London, 2002.
[6] Z.P. Bažant, S. Beissel, Smeared-tip superposition method for cohesive fracture with rate effect and creep, Int. J. Fract. 65 (1994) 277–290.
[7] Z.P. Bažant, L. Cedolin, Stability of Structures: Elastic, Inelastic, Fracture, and Damage Theories, Oxford University Press, New York, 1991; and 2nd ed., Dover Publications, New York, 2003.
[8] Z.P. Bažant, Y.-N. Li, Stability of cohesive crack model: Part I—Energy principles, J. Appl. Mech. ASME 62 (1995a) 959–964.
[9] Z.P. Bažant, Y.-N. Li, Stability of cohesive crack model: Part II—eigenvalue analysis of size effect on strength and ductility of structures, J. Appl. Mech. ASME 62 (1995a) 965–969.
[10] Z.P. Bažant, E.P. Chen, Scaling of structural failure, Appl. Mech. Rev. ASME 50 (10) (1997) 593–627.
[11] Z.P. Bažant, J. Planas, Fracture and Size Effect: in Concrete and Other Quasibrittle Materials, CRC Press, New York, 1998.
[12] Z.P. Bažant, I.M. Daniel, Z. Li, Size effect and fracture characteristics of composite laminates, J. Eng. Mater. Technol. ASME 118 (3) (1996) 317–324.
[13] Z.P. Bažant, J.H. Kim, I.M. Daniel, E. Becq-Giraudon, G. Zi, Size effect on compression strength of fiber composites failing by kink-band propagation, Int. J. Fract. 95 (1999) 103–141.
[14] B. Budiansky, Micromechanics, Comput. Struct. 16 (1–4) (1983) 3–12.
[15] N.A. Fleck, Compressive failure of fiber composites, Adv. Appl. Mech. 33 (1997) 43–117.
[16] N.A. Fleck, S. Sivashanker, M.P.F. Sutcliffe, Compressive failure of composites due to microbuckle growth, Eur. J. Mech. Solids 16 (1997) 65–82.
[17] G.V. Guinea, J. Planas, M. Elices, Correlation between the softening and the size effect curves, in: H. Mihashi, H. Okamura, Z.P. Bažant (Eds.), Effect in Concrete Structures, E&FN Spon, London, 1994, pp. 233–244.
[18] G.V. Guinea, M. Elices, J. Planas, On the initial shape of the softening function of cohesive materials, Int. J. Fract. 87 (1997) 139–149.
[19] A. Hillerborg, Numerical methods to simulate softening and fracture of concrete, in: G.C. Sih, A. DiTomasso (Eds.), Fracture Mechanics of Concrete: Structural Application and Numerical Calculation, Martinus Nijhoff, Dordrecht, 1985, pp. 141–170, 33, 43–117.
[20] A. Hillerborg, M. Modéer, P.E. Petersson, Analysis of crack formation and crack growth in concrete by means of fracture mechanics and finite elements, Cement Concrete Res. 6 (1976) 773–782.
[21] Y.-N. Li, Z.P. Bažant, Eigenvalue analysis of size effect for cohesive crack model, Int. J. Fract. 66 (1994) 213–226.
[22] Y.-N. Li, A.P. Hong, Prediction of failure in notched infinite strips by the cohesive crack model, Int. J. Solids Struct. 29 (23) (1992) 2815–2828.
[23] Y.-N. Li, R.Y. Liang, The theory of boundary eigenvalue problem in the cohesive crack model and its application, J. Mech. Phys. Solids 41 (2) (1993) 331–350.
[24] P.M. Moran, X.H. Liu, C.F. Shih, Kink-band formation and band broadening in fiber composites under compressive loading, Acta Metall. Mater. 43 (8) (1995) 2943–2958.
[25] P.E. Petersson, Crack growth and development of fracture zone in plain concrete and similar materials, Report no. TVBM-1006, Division of Building Materials, Lund Institute of Technology, Lund, Sweden, 1981.
[26] J. Planas, G.V. Guinea, M. Elices, Generalized size effect equation for quasibrittle materials, Fatigue Frac. Eng. Mater. Struct. 20 (5) (1997) 671–687.
[27] M.P.F. Sutcliffe, N.A. Fleck, Microbuckle propagation in carbon fibre-epoxy composites, Acta Metall. Mater. 42 (7) (1994) 2219–2231.
[28] H. Tada, P.C. Paris, G.R. Irwin, The Stress Analysis of Cracks Handbook, Del Research Corp., Hellertown, PA, 1985.